Langmuir
Article
pubs.acs.org/Langmuir

Dynamic Perspective on the Function of Thermoresponsive Nanopores from in Situ AFM and ATR-IR Investigations

Ana Maria Popa,*[,†,§] Silvia Angeloni,[†,‡] Thomas Bürgi,[‡,∥] Jeffrey A. Hubbell,[§] Harry Heinzelmann,[†] and Raphaël Pugin[†]

[†]*Centre Suisse d'Electronique et de Microtechnique SA, Rue Jaquet Droz 1, CH-2000 Neuchâtel, Switzerland,* [‡]*Institut de Chimie, Faculté des Sciences, Université de Neuchâtel, Rue Emile Argand 11, CH-2007 Neuchâtel, Switzerland,* [§]*Institute of Bioengineering and Institute of Chemical Sciences and Engineering, Ecole Polytechnique Fédérale de Lausanne (EPFL), CH-1015 Lausanne, Switzerland, and* [∥]*Physikalisch-Chemisches Institut, Universität Heidelberg Im Neuenheimer Feld 253, D-69120 Heidelberg, Germany*

Received June 29, 2010. Revised Manuscript Received August 24, 2010

This article describes the morphological and chemical characterization of stimuli-responsive functionalized silicon surfaces provided in parallel by atomic force spectroscopy (AFM) and Fourier transform infrared spectroscopy (FT-IR) enhanced by the single-beam sample reference attenuated total reflection method (SBSR-ATR). The stimuli-responsive behavior of the surfaces was obtained by grafting-to in melt carboxyl-terminated poly-*N*-isopropylacryl amides (PNIPAAM) with different degree of polymerization (DP) on epoxide-functionalized silicon substrates. The unprecedented real time and in situ physicochemical insight into the temperature-triggered response of the densely packed superficial brushes allowed for the selection of a PNIPAAM with a specific DP as a suitable polymer for the fabrication of silicon membranes exhibiting switchable nanopores. The fabrication process combines the manufacture of nanoporous silicon surfaces and their subsequent chemical functionalization by the grafting-to in melt of the selected polymer. Then, relevant information was obtained in what concerns the chemical modifications behind the topographical changes that drive the functioning of PNIPAAM-based hybrid nanovalves as well as the timescale on which the opening and closing of the nanopores occur.

Introduction

Nanopumps and nanovalves based on nanoporous membranes grafted with responsive polymers find applications in microfluidic sensors,[1,2] controlled-delivery systems,[3] and switchable filtration devices. The reversible intelligent opening and closing of the nanopores can be achieved by triggering a conformational change in the grafted polymer upon exposure to an external stimulus, such as a change in temperature,[4] light,[5] pH,[6] or electric potential.[7]

Temperature is one of the most relevant stimuli for biomedical applications because it is a parameter that can be adjusted within a wide value range in a noninvasive manner. This justifies the strong interest in the synthesis of water-soluble amphiphilic polymers containing pendant amphiphilic groups such as amide[8,9] or ether[10] that display a coil-to-globule transition upon an increase in their solution temperature above a critical value, the lower critical solution temperature (LCST). Among these polymers, poly-*N*-isopropylacryl amide (PNIPAAM) is probably the most widely used because its LCST (32 °C) is in the physiological range.

A number of studies have reported the immobilization of PNIPAAM on suitably functionalized nanostructured substrates such as nanoporous colloidal films,[11] track-etched poly(ethylene terephtalate)[12] and polycarbonate membranes,[13] PTFE microporous membranes,[14] and copper grids.[15] The response time of such switchable nanoporous supports depends on the membrane characteristics (i.e., thickness and porosity) but also on the features of the grafted polymer layer, namely, the grafting density, the chain length, and the changes in surface chemistry upon transition.

There are a vast number of reports concerning the grafting of such stimuli-responsive polymers on surfaces, with some excellent reviews on the subject published in the last few years.[16,17] Densely grafted brushes with excellent thickness control (narrow polydispersity) were obtained by performing controlled radical polymerization from immobilized initiator layers.[18−21] An alternative method to obtaining such dense layers is the grafting of presynthesized macromolecules in the solid state on suitably functionalized

*Corresponding author. Current address: Laboratory for Protection and Physiology, EMPA, CH-9014 St. Gallen, Switzerland. E-mail: ana-maria.popa@empa.ch.

(1) Chu, L.-Y.; Liang, Y.-J.; Chen, W.-M.; Ju, X.-J.; Wang, H.-D. *Colloids Surf., B* **2004**, *37*, 9–14.
(2) Li, Z.; He, Q.; Ma, D.; Chen, H. *Anal. Chim. Acta* **2010**, *665*, 107–112.
(3) Ito, T.; Yamaguchi, T. *Langmuir* **2006**, *22*, 3945–3949.
(4) Wang, C.; Stewart, R. J.; Kopecek, J. *Nature* **1999**, *397*, 417–420.
(5) Suzuki, A.; Tanaka, T. *Nature* **1990**, *346*, 345–347.
(6) Kiser, P. F.; Wilson, G.; Needham, D. *Nature* **1998**, *394*, 459–462.
(7) Khutoryanskaya, O. V.; Mayeva, Z. A.; Mun, G. A.; Khutoryanskiy, V. V. *Biomacromolecules* **2008**, *9*, 3353–3361.
(8) Heskins, M.; Guillet, J. E. *J. Macromol. Sci. Chem* **1968**, 1441–1455.
(9) Kirsh, Y. E.; Yanul, N. A.; Popkov, Y. M. *Eur. Polym. J.* **2002**, *38*, 403–406.
(10) Spěváček, J.; Starovoytova, L.; Hanyková, L.; Kouřilová, H. *Macromol. Symp.* **2008**, *273*, 17–24.
(11) Schepelina, O.; Zharov, I. *Langmuir* **2007**, *23*, 12704–12709.
(12) Geismann, C.; Yaroshchuk, A.; Ulbricht, M. *Langmuir* **2007**, *23*, 76–83.
(13) Lue, S.; Hsu, J.; Chen, C. *J. Membr. Sci.* **2007**, *301*, 142–150.
(14) Han, C.-C.; Wei, T.-C.; Wu, C.-S.; Liu, Y.-L. *J. Membr. Sci.* **2010**, *358*, 60–66.
(15) Song, W.; Xia, F.; Bai, Y.; Liu, F.; T., S.; Jiang, L. *Langmuir* **2007**, *23*, 327–331.
(16) Prakash, S.; Karacor, M. B.; Banerjee, S. *Surf. Sci. Rep.* **2009**, *64*, 233–254.
(17) Goddard, J. M.; Hotchkiss, J. H. *Prog. Polym. Sci.* **2007**, *32*, 698–725.
(18) Millard, P.-E.; Mougin Nathalie, C.; Böker, A.; Müller Axel, H. E. In *Controlled/Living Radical Polymerization: Progress in ATRP*; American Chemical Society: Washington, DC, 2009; pp 127−137.
(19) Mittal, V.; Matsko, N. B.; Butté, A.; Morbidelli, M. *Eur. Polym. J.* **2007**, *43*, 4868–4881.
(20) Jones, D. M.; Smith, J. R.; Huck, W. T. S.; Alexander, C. *Adv. Mater.* **2002**, *14*, 1130–1134.
(21) Kizhakkedathu, J. N.; Norris-Jones, R.; Brooks, D. E. *Macromolecules* **2004**, *37*, 734–743.

surfaces at temperatures above the polymer's glass-transition point. In particular, the pioneering work of Tsukruk and Stamm dealt with the grafting of functional polymers in the molten state on epoxide-functionalized surfaces or epoxide-functionalized polymer layers, showing the possibility to obtain high-density brushes. Hydrophobic,[22,23] hydrophilic,[24] and mixed brushes[25] were synthesized by this grafting-to in melt method. Yim et al. had already emphasized the importance of using densely packed brushes of high-molecular-weight PNIPAAM to trigger the responsive behavior of carboxyl-terminated PNIPAAM grafted-to in melt on bare silicon.[26] The possibility of obtaining an epoxide-mediated grafting-to in melt approach to responsive polymers inspired this work. Flat silicon surfaces were functionalized using an epoxysilane as an anchoring layer to graft carboxyl-terminated PNIPAAM in the molten state. The introduction of the epoxysilane intermediate layer in our case greatly enhanced the density of the polymer brushes displaying the required stretched conformation to express the coil-to-globule transition fully. The same synthesis approach was used to graft PNIPAAM onto a nanostructured substrate with the aim of exploiting the coil-to-globule transition to switch a smart nanovalve reversibly.

To monitor the various morphological aspects of the temperature-dependent collapse of PNIPAAM layers, different methods have been used such as quartz crystal microbalance,[27] surface plasmon resonance,[28] neutron reflectivity,[29] ellipsometry,[30] sum-frequency-generated spectroscopy,[31] and atomic force microscopy (AFM).[32−34] Among these methods only the last one provides the necessary lateral resolution for investigating in situ the morphological modifications that accompany the opening and closing of smart pores.

For the in situ observation of the inherent chemical modifications of the surface conditioned by responsive polymers, few methods have been described. Recently, the responsive behavior of as-deposited PNIPAAM layers was studied by attenuated total reflection spectroscopy, ATR-FT-IR.[35,36] An IR-based approach introduced by Fringeli,[37,38] reported as single-beam sample reference (SBSR) ATR spectroscopy, is a powerful extension of existing methodologies and was applied in this work. This technique converts a conventional single-beam spectrometer into a pseudo-double-beam mode by mechanically adjusting the vertical position of the internal reflection element (IRE) so that the sample and reference can be measured almost at the same time. The usual time delay between the measurement of the reference and sample can be minimized, thus compensating for the instrumental drift, the environmental fluctuations, and/or contamination as well as the intrinsic modifications of the sample and eventually of the supporting crystal. Moreover, the sample and reference have the same thermal history. The SBSR-ATR setup presents a clear advantage when looking for signals related to the evolving events on the surface, as is the case for "smart" polymeric chains that participate in different chemical interactions when exposed to external stimuli. This method greatly enhances the understanding of the response mechanism of covalently grafted thermoresponsive polymer brushes, and subsequently of functionalized nanopores, but to our knowledge no reports exist on its application ex situ or in situ for this purpose.

Finally, the morphological changes in the PNIPAAM-functionalized silicon surfaces, exposed to temperatures above and below the LCST, were monitored in situ by dynamic-mode AFM, and the temperature-driven modification of the associated chemical conformational changes was monitored in situ by SBSR-ATR. Under these conditions, we could resolve by direct observation the contributions of the backbone structure and the intra- and intermolecular hydrogen bond formation and the disruption to the temperature-driven coil−globule transition of the grafted polymer. This parallel and unprecedented physicochemical understanding of the smart behavior of silicon surfaces bearing densely packed PNIPAAM brushes encouraged us to use the same grafting-to in melt chemistry to functionalize anisotropic silicon nanopores. In this way, we could provide them with an opening/closing switchable mechanism that represents the first step toward the fabrication of functional intelligent nanovalves. The response mechanism of the thermoresponsive nanopores was monitored by AFM in real time. Chemical and morphological insight into the behavior of the smart nanopores constitutes a base for the future rational design of nanovalves, nanopumps, and nanoscale actuators.

Experimental Section

Materials and Methods. The surfaces used for polymer immobilization were 10 mm × 10 mm flat silicon ⟨100⟩ chips (Si-Mat, Germany) and nanostructured silicon chips of the same size. The nanostructuring process leading to the fabrication of silicon substrates displaying 80 nm pores with a controlled surface/hole ratio is described elsewhere.[39] Because internal reflection elements (IRE) for the SBSR-ATR analysis were used, we obtained silicon (Si) prisms with a trapezoidal shape (50 mm × 20 mm × 2.0 mm, nominal angle of incidence $\theta = 45°$, 21 internal reflections, Komlas, Germany). Glycidylpropyloxytrimethoxysilane (GPS) was purchased from Aldrich, Switzerland and was dissolved as received in toluene (Riedel den Haen). The grafting reactions were conducted using carboxy-terminated poly-*N*-isopropylacrylamide (PNIPAAM-COOH) of various molecular weights (M_w = 66 400, 45 200, and 8800 g/mol with PIs of 1.35, 1.5, and 1.45, respectively; Polymer Source, Canada). We will refer to these polymers as PNIPAAM588, PNIPAAM400, and PNIPAAM78, with the number representing the corresponding degree of polymerization (DP). Solutions of these polymers were prepared in tetrahydrofuran (THF; Aldrich, Switzerland) to a final concentration of 10 mg/mL. All other solvents (dimethylformamide

(22) Iyer, K. S.; Zdyrko, B.; Malz, H.; Pionteck, J.; Luzinov, I. *Macromolecules* **2003**, *36*, 6519–6526.
(23) Luzinov, I.; Julthongpiput, D.; Malz, H.; Pionteck, J.; Tsukruk, V. V. *Macromolecules* **2000**, *33*, 1043–1048.
(24) Ionov, L.; Zdyrko, B.; Sidorenko, A.; Minko, S.; Klep, V.; Luzinov, I.; Stamm, M. *Macromol. Rap. Commun.* **2004**, *25*, 360–365.
(25) Minko, S. *ACS Symp. Ser.* **2007**, *957*, 79–93.
(26) Yim, H.; Kent, M. S.; Mendez, S.; Lopez, G. P.; Satija, S.; Seo, Y. *Macromolecules* **2006**, *39*, 3420–3426.
(27) Ma, H.; Fu, L.; Li, W.; Zhang, Y.; Li, M. *Chem. Commun.* **2009**, *23*, 3428–3430.
(28) Balamurugan, S.; Mendez, S.; Balamurugan, S. S.; O'Brie, M. J.; Lopez, G. P. *Langmuir* **2003**, *19*, 2545–2549.
(29) Yim, H.; Kent, M. S.; Huber, D. L.; Satija, S.; Majewski, J.; Smith, G. S. *Macromolecules* **2003**, *36*, 5244–5251.
(30) Kurz, V.; Grunze, M.; Koelsch, P. *ChemPhysChem* **2010**, *11*, 1425–1429.
(31) Schmaljohann, D.; Nitschke, M.; Schulze, R.; Eing, A.; Werner, C.; Eichhorn, K.-J. *Langmuir* **2005**, *21*, 2317–2322.
(32) Kidoaki, S.; Ohya, S.; Nakayama, Y.; Matsuda, T. *Langmuir* **2001**, *17*, 2402–2407.
(33) Callewaert, M.; Grandfils, C.; Boulangé-Petermann, L.; Rouxhet, P. G. *J. Colloid Interface Sci.* **2004**, *276*, 299–305.
(34) Ishida, N.; Kobayashi, M. *J. Colloid Interface Sci.* **2006**, *297*, 513–519.
(35) Percot, A.; Zhu, X. X.; Lafleur, M. *J. Polym. Sci.., Part B: Polym. Phys.* **2000**, *38*, 907–915.
(36) Katsumoto, Y.; Tanaka, T.; Sato, H.; Ozaki, Y. *J. Phys. Chem. A* **2002**, *106*, 3429–3435.
(37) Fringeli, U. P.; Baurecht, D.; Günthard, H. H. In *Infrared and Raman Spectroscopy of Biological Materials*; Gremlich, H. U., Yan, B., Eds.; Marcel Dekker: New York, 2000; pp 143−192.
(38) Fringeli, U. P.; Baurecht, D.; Siam, M.; Reiter, G.; Schwarzott, M.; Bürgi, T.; Brüesch, P. In *Handbook of Thin Film Materials*; Nalwa, H. S., Ed.; Academic Press: New York, 2001; Vol. *2*, pp 191−229.
(39) Popa, A. M.; Niedermann, P.; Heinzelmann, H.; Hubbell, J. A.; Pugin, R. *Nanotechnology* **2009**, *20*, 485303.

(DMF), isopropanol, and *o*-xylene) were purchased from Aldrich, Switzerland, and used as received.

Substrate Cleaning and Activation. The flat silicon surfaces were cleaned by sonication in isopropanol (10 min) and were blown dry with nitrogen. This was followed by sample activation through 10 min of boiling in piranha solution (H_2SO_4/H_2O_2 2:1) and subsequent rinsing with Milli-Q water. ***Caution!*** *Piranha solution is a corrosive reagent that is prone to violent explosions when in contact with organic solvents and should be treated with care.*

The nanoporous surfaces were fabricated by transferring a self-assembled porous pattern onto the silicon substrate by deep reactive ion etching (DRIE) in a pulsed process using SF_6 as a reactive gas, C_4F_8 as a passivating agent, and a chromium pattern as an etching mask.[39] This process, known as the Bosch process, involves both the etching of the substrate and the formation of a passivation layer to allow the anisotropic etching of high-aspect-ratio nanopores with vertical side walls. For this reason, the activation procedure of nanostructured silicon involved supplementary cleaning steps after sonication. In the first step, the samples were exposed to O_2 plasma (1000 W, 3 min) in order to remove the fluorinated polymers deposited during the passivation step. The samples were then immersed in a chromium wet-etch solution for 3 min to eliminate any residues of the metallic mask. They were further activated by immersion in piranha solution as previously described.

The Si prisms used for the ATR analysis were first polished with a 0.25 μm grain size diamond paste (Buehler, Metadi II) and rinsed with ethanol before the surface was plasma cleaned under a flow of air for 5 min. To reproduce accurately the conditions propitious to the chemical functionalization carried out on the ⟨100⟩ flat and nanostructured silicon chips, the Si IREs were treated in the same way as described above. All samples were blown dry with nitrogen and immediately submitted to functionalization.

Substrates Functionalization with GPS. The ⟨100⟩ flat, nanostructured chips and the IRE were immersed for 13 h in a 1% (v/v) solution of GPS in toluene. The environmental humidity at the time of the experiment was estimated to be around 15%. After the reaction, the slides were rinsed with toluene and isopropanol and immediately coated with the polymeric films.

Polymer Film Deposition and Grafting-To in Melt. Thin films of PNIPAAM588, PNIPAAM400, and PNIPAAM78 were deposited onto the epoxy-functionalized surfaces by spin coating 10 mg/mL THF solutions of the respective polymer at spin speeds ranging from 2000 to 6000 rpm. The samples were then placed in a vacuum oven at 170 °C for 7 h. This procedure was applied for series A. Flat Si chips were submitted to the same procedure without annealing, as control 1 (C1). PNIPAAM films were cast on hydrophilic, bare, flat Si chips and annealed as control 2 (C2).

After being annealed, the substrates were cooled under nitrogen to room temperature, extracted with cold DI water, and sonicated in THF and DMF in order to remove the noncovalently grafted polymeric chains. The Si IREs were designed to be compatible with the SBSR technique; therefore, they needed to be functionalized only on half of the shorter surface of the prism. This area was denoted as the sample (S) area and corresponded to the upper part of the prism when mounted into the FT-IR spectrometer measurement compartment. The other half of the functionalized prism surface was cleaned with an ethanol wet pad to remove the cast NIPAAM just before starting the annealing process.

Ellipsometric Measurements. Ellipsometric measurements were performed on the flat samples using a spectroscopic ellipsometer (Jobin Yvon, France) at an angle of incidence of 70°. The instrument is equipped with a monochromator that allows the variation of the incident wavelength, and for the experiments performed in this work, the latter was varied between 400 and 800 nm in increments of 20 nm. The modeling steps were performed using DeltaPsi2 software (Jobin Yvon, France). The initial silicon samples and samples functionalized with the anchoring silane layer were measured independently and used as a reference. A tri-layer model was used to simulate the silicon substrate + silicon dioxide layer + polymer film. The refractive indices for the thee layers were as follows: SiO_2 = 1.5, GPS = 1.429,[23] and PNIPAAM-COOH = 1.45.[40]

The distance between adjacent chains D was calculated from

$$D = \left(\frac{4}{\pi \sum}\right)^{1/2} \tag{1}$$

where Σ, the grafting density, is calculated from

$$\sum = \frac{\Gamma N_A \times 10^{-21}}{M_w} \tag{2}$$

where N_A is Avogadro's number and M_w is the weight-average molecular weight of the polymer chains.

The surface coverage Γ is calculated from

$$\Gamma = h\rho \tag{3}$$

where h is the measured thickness and ρ is the density; here we assume a bulk density of PNIPAAM of 1.07 g/cm^3[40]

X-ray Photoelectron Spectroscopy (XPS). The XPS analysis was performed using a Kratos Axis Ultra spectrometer equipped with a concentric hemispherical analyzer in the standard configuration. All of the spectra were acquired using a monochomatic Al Kα mono (1486.6 eV) X-ray radiation source operated at 15.0 kV and 150 W in ultrahigh vacuum (base pressure below 10^{-9} mbar). The acquired data was analyzed using CasaXPS software.

Tapping-Mode AFM in Air. The tapping-mode AFM in air measurements were conducted on Dimension 3100 equipment (Veeco Digital Instruments) equipped with a Nanoscope IIIa controller (Veeco). The typical probes used were aluminum-coated cantilevers with silicon nitride tips having a radius of less than 10 nm (Budgetsensors).

Tapping-Mode AFM in a Liquid. The AFM in liquid measurements were carried out on a Nanowizard II JPK instrument (JPK, Berlin, Germany) equipped with a temperature-controlled microfluidic cell (Biocell). The probe used was a CSC37 silicon cantilever (lever C) without an aluminum coating from MikroMash with a resonance frequency in air of 40 kHz. The resonance frequency in water was 14.4 kHz. The tip curvature radius, which was less than 10 nm, was given by the manufacturer. The stiffness, k = 0.08 nN/nm, has been determined by thermal calibration. All of the experiments have been performed in Milli Q water (18.2 MΩ). The images have been analyzed using JPK Image Software.

Single-Beam Sample Reference (SBSR) ATR FT-IR Spectroscopy. ATR-IR measurements were performed on a Bruker Equinox 55 FT-IR spectrometer equipped with a nitrogen-cooled narrow-band mercury−cadmium−telluride (MCT) detector and a lift-model SBSR-ATR mirror attachment (OptiSpec). Spectra were recorded at a resolution of 4 cm^{-1}. A wire grid polarizer was used to generate linearly polarized light parallel and perpendicular to the plane of incidence. SBSR analyses imply that one-half of the IRE was dedicated to the sample (S) and the other half was dedicated to the reference (R). As consequence of the functionalization design, the number of active internal reflections containing chemical information is N = 10 for the functionalized IRE. The two sides of the IRE were separately addressed with flow-through cells. The temperature of the cell was measured with a thermocouple and was controlled using a water circulation system connected to a thermostat. Measurements were performed using the SBSR lift accessories, namely, a computer-controlled lifting mechanism for alternatively aligning the sample S or the

(40) Tu, H.; Heitzman, C. E.; Braun, P. V. *Langmuir* **2004**, *20*, 8313–8320.

Table 1. Ellipsometric Thickness of the Synthesized PNIPAAM Brushes as a Function of DP[a]

	ellipsometric thickness (nm)		
DP	A	C1	C2
78	4.1 ± 0.5	0.2	0.9
400	10.2 ± 0.3	0.3	1.9
588	15.6 ± 0.7	0.4	4.6

[a] (A) Silanized and annealed samples; (C1) silanized sample, not annealed; (C2) silane-free annealed sample. Each experiment was carried in triplicate; the control experiments were carried only once.

reference R with the IR beam. Water and CO_2 were removed from the spectrometer beam path using an air purging system. The spectrometer and accessories were controlled with OPUS software (Bruker).

Results and Discussion

Fabrication of PNIPAAM Brushes on Silicon Surfaces by the Grafting-To in Melt Method. Three series of experiments were performed in order to assess the strength of interaction between PNIPAAM-COOH chains of different lengths and the epoxy silane (GPS)-functionalized surfaces. Experimental series A consisted of the annealing of the polymer at 170 °C on surfaces functionalized with GPS. Series C1 is the first control experiment designed to assess the grafting ability of the epoxy silane at room temperature by skipping the annealing step. Series C2 is the second control experiment that involved the PNIPAAM film annealing on bare hydrophilic silicon surfaces in order to evaluate the ability of PNIPAAM to interact with silanol groups of the substrate at high temperature by skipping the formation of the epoxide intermediate layer. A series of preliminary experiments have shown that the thickness of a covalently grafted layer of PNIPAAM increases sharply with the annealing time, reaching saturation after 7 h. Therefore, that duration was chosen for all experiments described herein. The annealing temperature for the spin-coated films was chosen to be 170 °C, which is well above the T_g of PNIPAAM (132 °C)[41] and inferior to its thermal degradation temperature (350 °C).[41] The thickness of the layers was measured by ellipsometry in air and by SBSR-ATR in liquid. The ellipsometric thicknesses of the immobilized polymer layers in the dry state, at room temperature, as a function of the DP are summarized in Table 1. The epoxy silane layer thickness was found to be 4.2 ± 0.4 nm, which corresponds to about five monolayers. This is expected in the case of silane deposition without strict humidity control.[42]

The first observation is that the highest thicknesses relate to GPS-functionalized samples, which were also subjected to annealing (series A). Additionally, the thickness of the samples in series A increases with the molecular mass of the polymer used. In the case of functionalized samples that have not been annealed (C1), layer thicknesses inferior to 1 nm were found. This confirms, as expected, that the reaction rate between the epoxide-functionalized layer and the thermoresponsive macromolecules is low at room temperature. On the silane-free samples, thin layers of polymer were still present even after more sonication cycles in a good solvent for PNIPAAM. The observed dependence of the measured thickness on the molecular weight of the polymers suggests that during the annealing process the end-capping carboxylic groups react to some extent with the silanols on the surface; however, the yield of this reaction is much lower than for the one involving the opening of the epoxide ring.

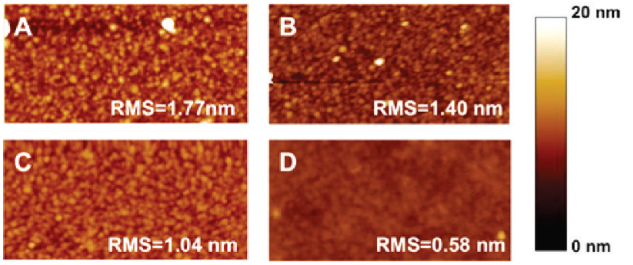

Figure 1. Roughness evaluation from AFM micrographs acquired in air on (A) a GPS layer and (B) PNIPAAM78, (C) PNIPAAM400, and (D) PNIPAAM588 grafted surfaces.

However, ellipsometry is an averaging method and cannot be reliably used for a grafting density assessment without a supplementary confirmation that the measured layers are indeed homogeneous on the nanometric level. We have therefore conducted an AFM analysis in air, at ambient temperature, on the stepwise-functionalized surfaces.

The analysis of the AFM images of the GPS layers (Figure 1A) allowed the determination of a mean roughness of about 1.77 nm for the anchoring layer, which is much lower than the film thickness calculated from the ellipsometric data. This observation confirms the obtaining of a homogeneous epoxy−silane layer. Upon PNIPAAM grafting, the rms amplitudes of tapping-mode AFM images decreased as the molecular weight of the polymer increased (Figure 1B−D). Additionally, these values were in all cases lower than the one observed for the GPS layer. This result, which was correlated with the lack of large aggregates on the analyzed areas, speaks to the fabrication of thick, uniform brushes by the grafting-to in melt approach. Finally, this first series of measurements showed that the introduction of the epoxide-functionalized layer greatly enhanced the grafting effectiveness.

The qualitative assessment of the conformation of the polymer chains (pancakelike, weakly/strongly stretched) in the grafted layer was realized by evaluating the ratio of the distance between two adjacent grafting sites (D) to the Flory radius (R_f) of the polymers.[43] The calculation of D is based on the polymeric brush height. If $D/2R_f$ is > 1, then the polymers are loosely grafted and flattened on the surface into a pancake conformation. $D/2R_f < 1$ is characteristic of weakly stretched brushes, where a small degree of overlap is present, and $D/2R_f \ll 1$ (below 0.1)[43] is characteristic of strongly stretched chains that form polymer brushes. It is noteworthy that the polymeric chain conformation depends not only on the grafting density but also on the quality of the solvent.[44] In the present case, we consider only the conformation adopted by the polymeric chains in a good solvent (PNIPAAM chains in water); therefore, the calculations were made using the value of the corresponding R_f, as deduced from eq 4

$$R_f = a(DP)^{3/5} \quad (4)$$

where a is the length of the statistical segment and was considered to be 0.3 (flexible polymers).

Investigations performed on the grafting-to in melt of other polymeric systems have shown that the degree of stretching increases with the molecular mass until the latter reaches values close to the critical entanglement molecular mass (M_c) and then

(41) Brandrup, J.; Immergut, E. H. *Polymer Handbook*; John Wiley & Sons: New York, 1989.
(42) Daniels, M. W.; Sefcik, J.; Francis, L. F.; McCormick, A. V. *J. Colloid Interface Sci.* **1999**, *219*, 351–356.
(43) Zhu, X.; Yan, C.; Winnik, F. M.; Leckband, D. *Langmuir* **2006**, *23*, 162–169.
(44) de Gennes, P. G. *Adv. Colloid Interface Sci.* **1987**, 27.

Table 2. Grafting Parameters for the Synthesized PNIPAAM Brushes[a]

DP	H (nm)	D (nm)	Σ (chains/nm^2)	Γ (mg/m^2)	R_f (nm)	$D/2R_f$	L (nm)
78	4.1	2.02	0.29	4.38	4.1	0.24	6.64
400	10.2	3.01	0.14	10.5	10.9	0.13	26.1
588	15.6	2.91	0.15	16.53	13.7	0.11	38.9

[a] H is the average ellipsometric thickness, D is the distance between two adjacent anchoring points as deduced from eq 1, Σ is the chain density calculated from eq 2, Γ is the surface coverage calculated from eq 3, R_f is the Flory radius for PNIPAAM calculated from eq 4, and L is the swollen thickness of the PNIPAAM chains in a good solvent calculated from eq 5. The $D/2R_f$ ratio relates to the degree of stretching of the polymer brush conformation.

decreases, reaching values of < 1 for high-M_w systems.[24] For the systems analyzed in this work, the maximum degree of stretching is observed for the highest molecular mass polymer, with a $D/2R_f$ value of almost 0.1, which is characteristic of stretched chains. The collected data correlate with densely grafted PNIPAAM chains.

Table 2 also includes the values of the length of the swollen polymeric chains in a good solvent (L), as can be deduced by introducing the determined distance between the grafting sites in the equation proposed by Alexander and De Gennes,[44,45]

$$L = \frac{M}{M_0} \times a \times \left(\frac{a}{D}\right)^{2/3} \quad (5)$$

where a is the statistical segment length, M is the average molecular weight of the polymer, M_0 is the molecular weight of the monomer, and D is the distance between two adjacent grafting sites.

The length of the swollen polymer is much higher than the calculated Flory radius. The difference can be attributed to a modification of the polymer layer thickness upon the stretching of individual molecules in a good solvent. However, the length of swollen PNIPAAM chains can be determined in a more quantitative manner from SBSR-ATR data directly acquired from PNIPAAM films immersed in liquid. The calculation in this case relies on the assumption that the quantitative volume concentration, c, and surface concentration, Γ, are related to each other via the thickness of the sample d and the Lambert−Beer law by eq 6.

$$c = \frac{\Gamma}{d} = \frac{A_\perp}{N v d_{e,\perp} \int \varepsilon(\tilde{\nu})\, d\tilde{\nu}} \quad (6)$$

$A_\perp$ denotes the integrated absorbance of a given absorption band measured with perpendicularly polarized light; N and v are the mean number of active internal reflections and the number of equal functional groups per molecule. The effective thickness of an arbitrarily oriented sample per internal reflection is denoted by $d_{e,\perp}$, whereas $d^{iso}_{e,\perp}$ is the effective thickness of an isotropic sample and $\int \varepsilon(\tilde{\nu})\, d\tilde{\nu}$ denotes the integrated molar absorption coefficient of this band. According to eq 6, the surface density, Γ, may be conceived as the projection on the surface of the molecules in the volume defined by the unit area and the height d. Consequently, d is the sample thickness. The detailed calculations are reported in the Supporting Information and benefit from the possibility of considering the surface distribution of the grafted polymer to be isotropic. They are based on the following set of data: 3.4 is the Si refractive index, 1.45 is the value of the thin film refractive index, 1.289 represents the water refractive index at the wavelength corresponding to the amide I absorption, also taking into account the wavelength dependence,[46,47] and 1.002×10^8 cm$^2 \cdot$mol^{-1} is the molar absorption coefficient experimentally measured (in dichloromethane) at 1655 cm^{-1}. The calculations were performed using a program developed by Fringeli and co-workers.[48−50] For the PNIPAAM588 films, the calculated thickness was 32 nm, which is relatively close to the value deduced from the Alexander−De Gennes eq (38 nm) and confirms the formation of dense polymeric layers by grafting-to in the molten state.

Temperature-Induced Morphological Changes of the PNIPAAM Grafted Surface Monitored in Situ by AFM. The responsiveness of the obtained brushes was analyzed by AFM in liquid media at temperatures below and above the LCST of PNIPAAM (32 °C). AFM is the method of choice for analyzing the morphological modifications of the functionalized surfaces, allowing reasonable vertical and lateral resolution. Additionally, this approach allows us to monitor the brush conformational changes in real time. To ensure the measurement's stability, a 10 min delay after reaching the temperature set point was rigorously respected. A software flattening procedure was applied to the acquired images in order to remove artificial offsets between consecutive scan lines.

The topography of the substrates functionalized with the lower-molecular-mass polymer did not suffer drastic changes upon heating (Figure 2A,B). Recent studies[43,51] have indeed shown that PNIPAM chains with fewer than 100 monomer units in the main chain do not display a temperature-dependent collapse because this is the minimum chain length that enables a cooperative conformation change. In a similar manner, no major increase in the surface roughness was observed in the case of the substrate grafted with the polymer having an intermediate DP (Figure 2C,D).

This is in good agreement with results previously obtained in our group for thermoresponsive brushes grafted on gold surfaces.[52] We have shown that although a modification of the elastic properties of densely grafted PNIPAAM brushes with an intermediate DP can be observed by dynamic AFM, no modifications of the surface morphology occur. The striking feature reported in Figure 2 is the morphology switching between smooth and rough upon heating the medium to temperatures greater than 32 °C as expressed by an rms increase in the topography of the PNIPAAM588-coated sample (E and F). Above the LCST, the formation of coalesced domains of about 15 nm in height was observed. To understand better the observed topography modification with increasing temperature, an analogy between the phenomenon observed in our system and the behavior of polymeric chains in poor solvents explained at the theoretical level by Halperin and Zhulina[53] can be made. The authors predicted several structural regimes for different solvent qualities, degrees of polymerization, and grafting densities. In poor solvents at very high grafting density, the brush retains lateral stability and no topography modification is expected. At low grafting density, the brush splits into separate globules in which the chains

(45) Alexander, S. *J. Phys.* (*Paris*) **1977**, *38*, 977.
(46) Bertie, J. E.; Ahmed, M. K. *J. Phys.Chem. B* **1989**, *93*, 2210–2218.
(47) Downing, H. D.; Williams, D. *J. Geophys. Res.* **1975**, *80*, 1656–1661.
(48) Schwarzott, M.; Engelhardt, H.; Klühspies, T.; Baurecht, D.; Naumann, D.; Fringeli, U. P. *Langmuir* **2003**, *19*, 7451–7459.
(49) Reiter, G.; Siam, M.; Falkenhagen, D.; Gollnerictsch, W.; Baurecht, D.; Fringeli, U. P. *Langmuir* **2002**, *18*, 5761–5771.
(50) Fringeli, U. P.; Goette, J.; Reiter, G.; Siam, M.; Baurecht, D. In *Fourier Transform Spectroscopy*; deHaseth, J. A., Ed. 1998; pp 729−747.
(51) Aseyev, V.; Tenhu, H.; Winnik, F. In *Conformation-Dependent Design of Sequences in Copolymers II*; Khokholov, A., Ed.; Springer: Berlin, 2006; pp 1−85.
(52) Montagne, F.; Polesel-Maris, J.; Pugin, R.; Heinzelmann, H. *Langmuir* **2008**, *25*, 983–991.
(53) Halperin, A.; Zhulina, E. B. *Macromolecules* **2002**, *24*, 5393–5397.

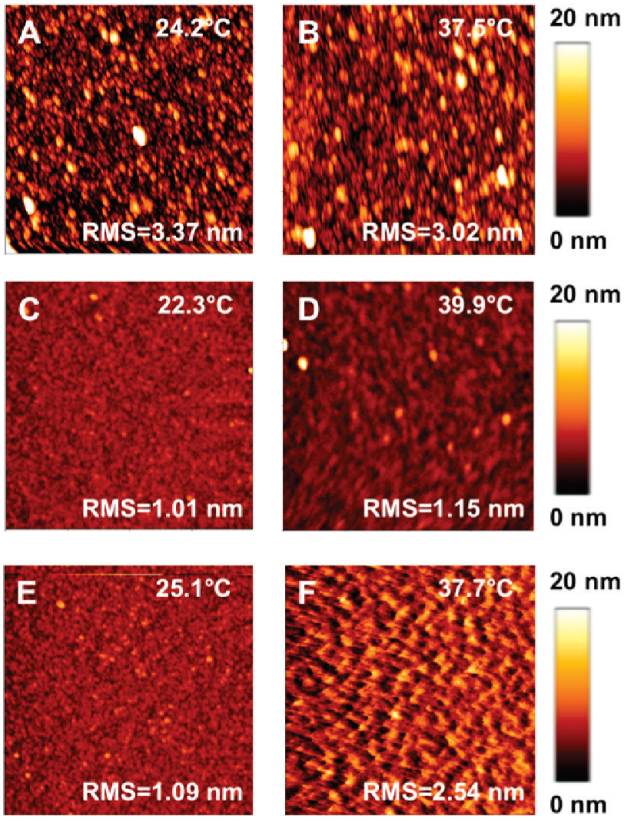

Figure 2. AFM micrographs (2 μm × 2 μm) acquired in liquid on flat substrates functionalized with PNIPAAM with different DPs. PNIPAAM78 (A) below and (B) above the LCST; PNIPAAM400 (C) below and (D) above the LCST; and PNIPAAM588 (E) below and (F) above the LCST.

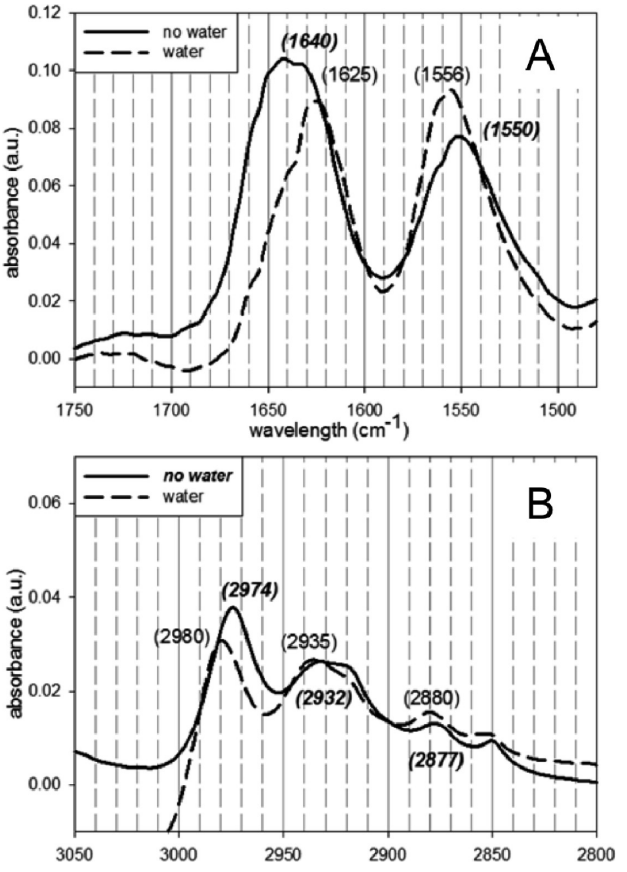

Figure 3. (A) Close-up of the optical range of the amide I and amide II absorption bands. (B) Close-up of the optical range of the methyl and methylene group stretching vibrations.

adopt a Gaussian conformation. This phenomenon was previously observed for the aggregation of long PNIPAAM chains adsorbed on glass surfaces that upon temperature switch collapse into the form of compact globules.[33] However, at moderate grafting densities separate globules can aggregate and form so-called pinned micelles. Ishida et al. also reported a similar behavior of PNIPAAM chains grafted from silicon wafers.[34] Therefore, it seems reasonable to expect comparable morphological switches also in the case of the PNIPAAM588 immobilized layer, since the layers of PNIPAAM display a grafting density at the inferior limit of the brush domain. At temperatures below the LCST, the macromolecular layer is swollen and homogeneously covers the underlying silane film. Upon temperature increase, the collapse of the polymeric chains leads to a 2-fold increase in the surface roughness, corresponding to the formation of coalesced domains of approximately 15 nm height.

According to these observations, PNIPAAM with a DP of 588 appears to be the most promising for the fabrication of thermoresponsive nanovalves. We therefore chose to investigate further the molecular conformation of brushes obtained from this particular system by SBSR-ATR in order to gain a deeper understanding of the phenomena that lead to temperature-related morphology modifications.

Temperature-Induced Molecular Conformational Changes of the PNIPAAM588 Grafted Silicon Surface Monitored in Situ by SBSR-ATR. To gain direct insight into the molecular conformational changes associated with the morphological switch of the PNIPPAM588-conditioned substrates, a silicon IRE exhibiting the same chemical properties of the flat, nanoporous silicon ⟨100⟩ chips and fulfilling the optical requirement of SBSR-ATR-IR spectroscopy was chemically modified according to the same grafting-to in melt method. The functionalized IRE was addressed through a microfluidic double cell, thus measuring in situ the spectra of the grafted PNIPAAM brushes when exposed to water at room temperature. First, we outlined the difference between the dry and wet states, and second, we could appreciate the temperature-driven responsiveness in water in real time. Available ATR data refer to PNIPAAM in solution or just cast on a support,[35,54] and to our knowledge, no FT-IR investigations have been conducted on covalently grafted PNIPAAM brushes. Two optical regions are of particular interest, one corresponding to the absorption of the amide groups (1800−1450 cm^{-1}) and one due to the absorption of the isopropyl/backbone methylene group (3000−2700 cm^{-1}). A close-up of these two optical regions is given in Figure 3A,B, respectively. The band slightly above 1700 cm^{-1} was attributed to the C═O stretching vibration of the terminal acid group (COO−R) of the PNIPAAM588 through which the covalent linkage to the epoxy ring occurs. Compared to the data reported in the literature, small spectral shifts were observed. In fact, we attribute the differences to the conformational hindering introduced into the polymer backbone from the covalent anchoring to the silicon IRE. The amide I band above 1600 cm^{-1} contains the contribution of the C═O stretching vibration, and the amide II band (around 1550 cm^{-1}) is due to the coupled N−H bending and C−N stretching vibrations. The C═O group of an amide group of PNIPAAM can form hydrogen bonds with the N−H group of a neighboring

(54) Katsumoto, Y.; Tanaka, T.; Sato, H.; Ozaki, Y. *J. Phys. Chem. A* **2002**, *106*, 3429–3435.

amide group and/or with water. Upon H-bond formation, the amide I band shifts to a lower frequency whereas the amide II band is subjected to an upward shift. From Figure 3A we observe that when the polymer layer is in contact with water the amide I band shifts from 1640 (dry state) to 1625 cm^{-1} (water-filled chamber). The 15 cm^{-1} shift toward lower frequency is of the same order of magnitude and in the same direction as the difference in absorption observed for a cast film of a PNIPAAM not covalently linked (just adsorbed) in the dry state and an aqueous solution of PNIPAAM.[36] For the amide II band, an opposite shift is observed. The spectrum of the grafted PNIPAAM588 in the dry state shows a band at 1550 cm^{-1}. When the grafted polymer is exposed to water, the corresponding absorption is displaced to 1556 cm^{-1}. The values are again similar to those reported for a PNIPAAM cast film and a PNIPAAM aqueous solution.

The observations suggest that the C═O (amide I) and N−H (amide II) groups of the polymer side chains form hydrogen bonds and are hydrated in the aqueous solution. Another important difference between the two spectra is the relative intensity of the two bands and the fact that in the absence of water multiple bands can be observed in the amide regions. Both observations indicate different bonding interactions of the amide groups in the two situations.

Figure 3B displays the optical region of the methylene and methyl group stretching vibrations associated with the C−H stretching (ν_{C-H}) vibrations.[35,55] In the spectrum registered in the presence of water, the peaks at 2980 and 2880 cm^{-1} are assigned to the antisymmetric and symmetric ν_{C-H} of the methyl groups, respectively. The peak at 2935 cm^{-1} is attributed to the antisymmetric C−H stretching, ν_{C-H}, of the methylene groups of the polymer backbone. Compared to the homologue peaks registered in the absence of water, a consistent small shift was observed toward higher wavenumbers that was similar to that observed for the amide II band (Figure 3A) and thus can also be correlated with the modification of the backbone configuration.

The ν_{C-H} shift is therefore a useful probe for monitoring the temperature dependence of the organizational changes of alkyl chains because the CH_2 antisymmetric and symmetric stretching modes are sensitive to changes in the conformation of hydrocarbons chains.[56,57] A shift toward lower frequencies is in general interpreted as an increase in the conformational order during a transition even though other phenomena may be involved.[56,58]

Previous studies reported in the literature were carried out on thick PNIPAAM films deposited by solution casting on solid supports that are infrared-transparent (CaF_2).[36] In contrast, here we observed the responsive behavior of a thin PNIPAAM brush covalently grafted onto the surface of a silicon IRE. In this way, the parallelism between physical (AFM) and chemical characterization (IR) acquires significance. Furthermore, the responsive behavior triggered by temperature required an in situ technique that compensates for the modifications of the optical setup induced by temperature changes. In the absence of perfect compensation, the spectral change due to the temperature dependence of the refractive index of the IRE may overwrite the signals due to chemical effects (e.g., structural changes). The quasi-simultaneous registration by SBSR of the reference compartment exposed to the exactly same conditions as the sample compartment allowed for unprecedented compensation.

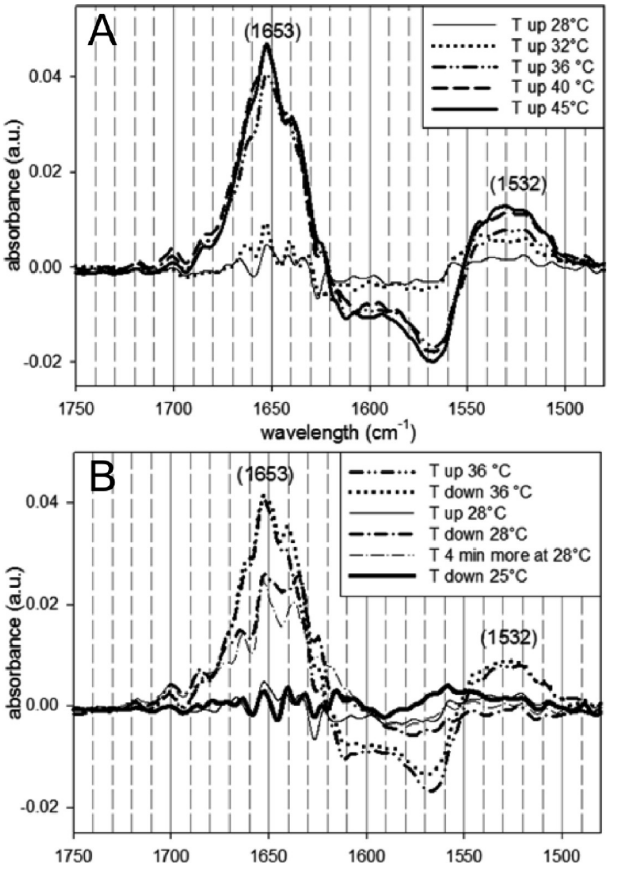

Figure 4. Close-up of the amide I and amide II optical regions of absorption for differential spectra registered first for (A) increasing (28, 32, 36, 40, and 45 °C) temperature steps and then for (B) decreasing temperature (36, 28, and 25 °C) steps. The spectra reported in graph B show the reversibility of the phenomena as well as the corresponding hysteresis for the amide I band.

Figure 4 depicts the close-up in the amide I and amide II absorption region of the SBSR-ATR differential spectra registered at different temperatures. The reported absorptions arise from the SBSR spectra registered at discrete temperatures minus the reference SBSR spectrum measured at 25 °C, thus providing access to the temperature-induced modifications. Five SBSR spectra were measured at 28, 32, 36, 40, and 45 °C upon heating, and afterwards three spectra at 36, 28, and 25 °C were obtained during subsequent cooling. Each measurement was initiated 4 min after temperature stabilization for every step.

The amide I band of PNIPAAM in aqueous solution contains three distinct contributions: the absorption of C═O involved in intermolecular hydrogen bonds with water that is observed at 1629 cm^{-1}, the absorption of C═O associated with a strong intramolecular hydrogen bond at 1655 cm^{-1}, and a higher-frequency absorption of about 1678 cm^{-1} related to free carbonyl.[35,55,59] These data correlate with the appearance upon heating of the particular absorption at 1653 cm^{-1} attributable to the increased number of C═O groups involved in intramolecular hydrogen bonding (Figure 4). The latter is partially responsible for the collapsed globule conformation. Although previously reported results rely on the fitting of deconvoluted peaks,[35] we could directly distinguish the contribution of the intramolecular hydrogen bond when exposing the polymer to water or when changing the temperature. The observed modifications indicate a

(55) Lin, S. Y.; Chen, K. S.; Liang, R. C. *Polymer* **1999**, *40*, 2619–2624.
(56) Kodati, V. R.; El-Jastimi, R.; Lafleur, M. *J. Phys. Chem.* **1994**, *98*, 12191–12197.
(57) Li, H.; Zhang, X.; Zhang, R.; Shen, J.; Zhao, B.; Xu, W. *Macromolecules* **1995**, *28*, 8178–8181.
(58) Umemura, J.; Cameron, D. G.; Mantsch, H. H. *J. Phys. Chem.* **1980**, *84*, 2272–2277.
(59) Skrovanek, D. J.; Painter, P. C.; Coleman, M. M. *Macromolecules* **1986**, *19*, 699–705.

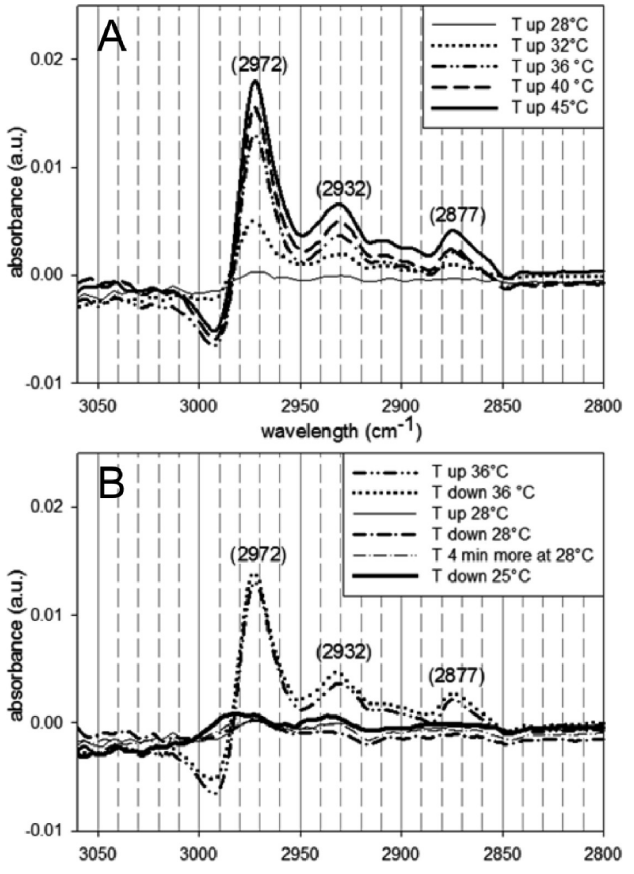

Figure 5. Close-up in the methyl/methylene optical region of absorption of differential spectra registered first for (A) increasing (28, 32, 36, 40, and 45 °C) temperature steps and then for (B) decreasing temperature (36, 28, and 25 °C) steps. The spectra reported in graph B show that for the backbone/isopropyl configuration the temperature transition is perfectly reversible.

change from intermolecular to intramolecular hydrogen bonds upon heating.

Moreover, a shift in the amide II region toward lower wavenumbers (from 1556 as reported in Figure 3A to 1532 cm^{-1} as reported in Figure 4) was observed. This peak is well outlined from the negative band registered that corresponds to the peak observed at constant temperature (1620−1550 cm^{-1} spectral range). The simple shift in frequency indicates that the amide II absorption is attributable only to a unique contribution, namely, to the degree of order of the backbone, and is not related to the modification of chemical bonds. Such behavior acquires relevance if considered in combination with the differential absorption bands registered in the 3050−2800 cm^{-1} spectral range reflecting the response of the C−H stretching vibrations of the isopropyl group towards a temperature gradient (25−45 °C, Figure 5). With increasing temperature, we observed the appearance of a negative signal centered at 2992 cm^{-1} and the emergence of a positive peak at 2972 cm^{-1}, which is almost at the same position as the antisymmetric methyl stretching vibrations ($\nu_{C-H,as}$) registered in the absence of water (2974 cm^{-1}, Figure 3B). For methyl $\nu_{C-H,as}$, we observed a global shift from 2980 cm^{-1} registered in water at room temperature (Figure 3B) to 2972 cm^{-1} with a change in temperature (Figure 5). The shift is of the same order of magnitude and in the opposite direction of the shift linked to the dry/wet transition state of the polymer. In fact, the same shifts, first to higher frequencies because of the wet/dry transition and then to lower frequencies upon the temperature

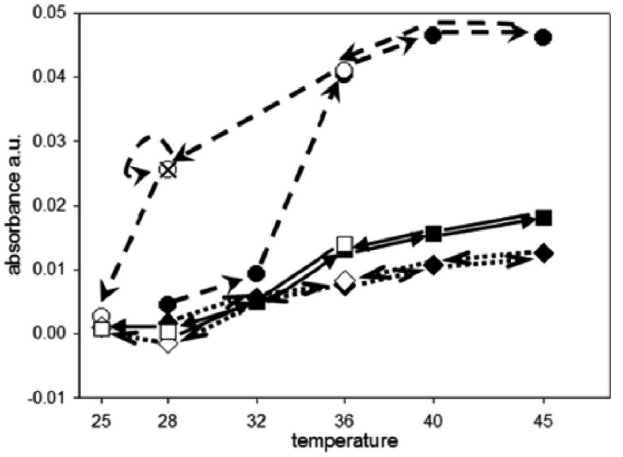

Figure 6. Schematic representation of the hysteresis observed for hydrogen bond formation/disruption. Discrete peak values belong to the spectra in Figures 4 and 5. ● represents differential peaks at 1653 cm^{-1} (amide I) in the increasing temperature path, and ○ represents the same peaks in the decreasing temperature path. × is the value of the peak at $T = 28$ after a supplementary 4 min of temperature stabilization. ♦ represents peaks at 1532 cm^{-1} (amide II) versus increasing temperature, and ◊ represents peaks at 1532 cm^{-1} (amide II) versus decreasing temperature. ■ and □ represent peaks at 2972 cm^{-1} (methyl $\nu_{C-H,\ as}$) versus increasing and decreasing temperature, respectively.

gradient effect, were observed for the peak belonging to the symmetric methyl vibration ($\nu_{C-H,s}$, 2877 cm^{-1} in the absence of water, 2880 cm^{-1} in the presence of water, and 2877 cm^{-1} upon TG, Figures 3B and 5). This was also the case for the antisymmetric methylene group stretching ($\nu_{C-H,as}$, 2932 cm^{-1} in the absence of water, 2935 cm^{-1} in the presence of water, and 2932 cm^{-1} upon TG, Figures 3B and 5).

The spectroscopic investigation by SBSR-ATR is extremely sensitive and allowed us to observe more subtle aspects of the reversible character of the transition process. In the case of the methyl/methylene groups, the spectra registered at the same temperature in ascending (Figure 5A) and descending (Figure 5B) directions are the same. The same consistent behavior was observed for amide II in Figure 4. Figure 4B also displays in the returning path (descending temperature) a certain hysteresis of the amide I band.

For this absorption again to reach the value obtained at $T =$ 28 °C with rising TG, it was not enough to decrease the temperature to 28 °C and wait the usual 4 min for stabilization. Even waiting 4 additional minutes had no effect. It was only when the temperature was further lowered to 25 °C that the same value was reached as was originally observed at 28 °C for the rising TG. The SBSR-ATR results suggest that the temperature transition is reversible but there is a temperature lag in the response of one of the two separated processes. Amide II and the methyl/methylene absorption (both sensitive to the backbone configuration) show consistent behavior whereas amide I, although reversibly sensitive to external stimuli, exhibits hysteresis that is probably due to a different recombination of the hydrogen bond back and forth with respect to the globule conformation.

In Figure 6 are reported the values of the differential absorbance varying according to the increasing and decreasing temperature at very specific wavelengths, namely, 1653, 1532, and 2972 cm^{-1}, respectively, which are representative of amide I (mainly related to the intramolecular hydrogen bond), amide II, and methyl stretching ν_{C-H}. The processed data are discrete points (absorbance values) extracted at the selected wavelength

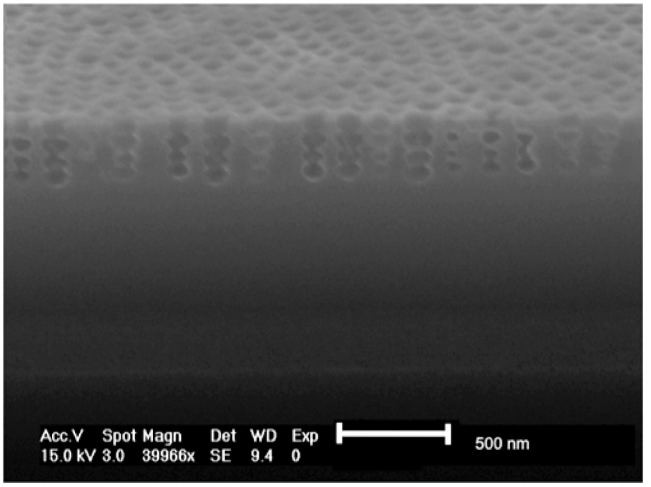

Figure 7. (SEM image) Side view of a nanoporous silicon surface on which a thin PNIPAAM588 layer was annealed for 7 h at 170 °C.

from the spectra already reported in Figures 4 and 5. The Figures reveal a hysteresis for the amide I band, in contrast to the amide II and C−H stretching bands. In other words, considering that amide I reflects hydrogen bond formation and disruption, a longer time is needed for the complete stabilization of chains through the newly reformed hydrogen bonds.

Fabrication of PNIPAAM588-Functionalized Nanoporous Surfaces and Characterization in Situ by AFM. The SBSR analysis of the chemical phenomena involved in globule formation confirmed the rapid occurrence of the transition process and provided information on its hysteretic nature. We therefore performed a proof-of-concept experiment and used the grafting-to in melt approach for the fabrication of thermoresponsive nanopores as a first step towards the fabrication of smart nanovalves with a high response rate.

We have previously described a versatile method for producing high-aspect-ratio nanopores in a silicon substrate by block copolymer lithography and showed the possibility of tuning their diameter and depth.[34] For this work, we have chosen a substrate with pores of about 80 nm in diameter, which are comparable to the size of the aggregates yielded by the PNIPAAM brushes upon collapse. A thin layer of PNIPAAM588 brushes was immobilized on the nanoporous silicon substrates by the described grafting-to in melt approach. To establish the extent to which the initial polymer film wets the interior/inside of the nanopores, some samples were manually cleaved after the annealing process and the exposed cross section was analyzed by SEM (Figure 7).

The image was acquired using a low-acceleration electron beam in order to avoid damaging the organic film. The thickness of the PNIPAAM layer after annealing was assessed on a flat surface and was found to be around 100 nm, which is much smaller than the depth of the nanopores (350 nm). The SEM analysis of the nanoporous substrate reveals that only the upper surface of the sample is homogeneously coated with the polymer film but the porous topography is still visible and some pores are empty in the cross section. We assume that only the topmost surface of the pores is homogeneously covered by the spin-coated polymer film and will as such be functionalized with the PNIPAAM brushes.

After the annealing and subsequent removal of unbound chains by means of extensive extraction and sonication cycles, the functionalized nanoporous surface was analyzed by AFM in liquid at temperatures below and above the transition temperature of the polymer. At 23.5 °C, the nanopores appear to be "open"; the average diameter of the functionalized nanopores, as

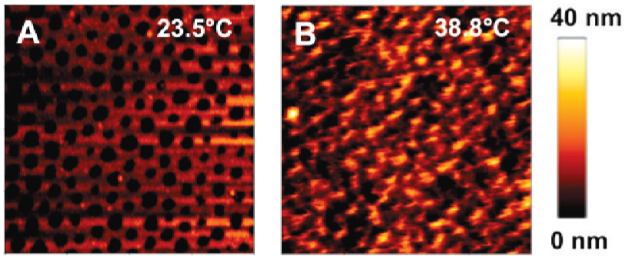

Figure 8. AFM micrographs (2 μm × 2 μm) acquired in liquid on nanoporous substrates functionalized with PNIPAAM58 (A) below and (B) above the LCTS.

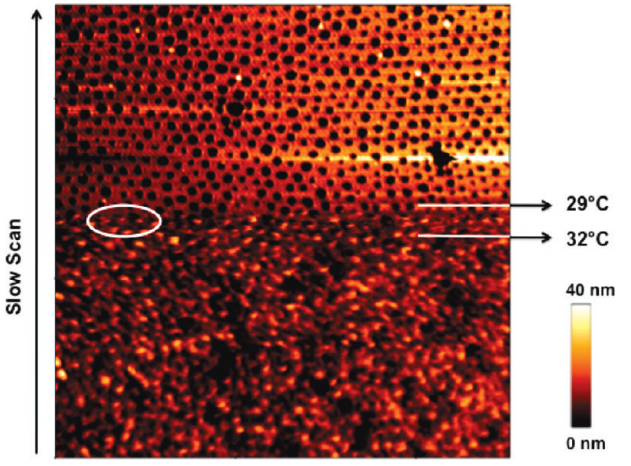

Figure 9. Real-time monitoring of the PNIPAAM588 chain collapse by tapping AFM in liquid media. The scan area is 4 μm × 4 μm.

determined from the analysis of the AFM images, was 80 nm, which is similar to that initially measured on the plain nanoporous substrates. Upon temperature increase, the surface morphology changed from "holey" to "bumpy" and the formation of aggregates with heights as great as 15 nm can be observed (Figure 8). This phenomenon closely resembles that observed on flat surfaces, and it seems to be independent of the presence of porous topography.

Previous studies have shown that a clear decrease in the elasticity of the immobilized PNIPAAM chains occurs when switching between the coil and globule states,[52] and this phenomenon is expected to influence the imaging process. The observed morphology modification of our nanopores can therefore be interpreted as follows: in the swollen state, the grafted polymer molecules are flexible and easily pushed away by the AFM tip, thus revealing the underlying porous topography. The cooperative collapse induced by the temperature increase leads to the formation of large, rigid globules that partially cover the pore openings and cannot be indented by the scanning probe.

To evaluate the switching time of such grafted layers, the temperature-induced transition of PNIPAAM588 was closely monitored by scanning a functionalized nanoporous surface while simultaneously sweeping the temperature between 37.8 and 24.3 °C. A larger image size and a higher scanning speed (2.5 kHz) were used to decrease the influence of the thermal drift. Figure 9 shows the result of such a measurement. The scanning direction is also shown.

The topography switching starts at 32.1 °C as indicated by the temperature sensor placed in the liquid at the sample level and ends at around 29 °C when the pores appear to be completely

open. The observed transition temperature is in good agreement with that observed for the functionalized flat surfaces. From the analysis of the transition area (circled in Figure 9), the gradual "covering" of the edges of the nanopores by the polymeric chains upon heating can be correlated with the formation of large aggregates of comparable size on the previously imaged flat surfaces (Figure 2). The in situ analysis of the thermally induced response also allowed us to calculate the transition time between different states for a given heating rate. From the available data on the scan rate and scan area, a transition time of 13 s was determined (details in Supporting Information). This result testifies to the rapid topographical response that nanopores functionalized with PNIPAAM brushes can display when subjected to temperature variations.

The changes in the polymer layer morphology with the temperature change have been reproducibly observed over more than 10 sweeping cycles performed in the same spot. This observation proves that the covalently attached chains can be reversibly switched between the hydrated and collapsed states without any delamination or dewetting phenomenon occurring. Upon heating the sample, however, a slight shift in the transition domain was observed: the collapsing of the polymer chains starting at around 32.4 °C and ending at around 34 °C, when the pores were considerably shrunken. This information confirms the hysteretic nature of the conformation change, previously noticed in the SBSR-ATR-IR experiments. However, in this case the process occurs only on a timescale of seconds and no considerable subcooling is needed to recover the initial topography. This demonstrates that the backbone conformation change of individual chains and the morphology change of the polymer brush are strictly interconnected whereas the recovery of the hydrogen bonds is clearly a decoupled process.

Conclusions

Dynamic AFM imaging in liquid allowed us to monitor the temperature-dependent morphological changes occurring on silicon surfaces functionalized with thermoresponsive PNIPAAM brushes of different molecular weights. The largest topography modification and increase in rms amplitude was observed for PNIPAAM588. The monitoring of the chemistry of PNIPAAM brushes in water, at different temperatures by SBSR-ATR-IR spectroscopy allowed the direct observation of two different chemical phenomena contributing to the brushes collapse: hydrogen bond formation−disruption, mainly affecting the amide I absorption, and the backbone configuration modification, predominantly affecting the amide II bands and the isopropyl methyl symmetric and antisymmetric C−H stretching vibrations as well as the antisymmetric vibrations of the methylene groups from the polymeric backbone. The hysteretic nature of the transition process was also put into evidence by SBSR-ATR.

We have also presented a proof of concept for the fabrication of thermosensitive nanopores by immobilizing PNIPAAM588 on nanostructured silicon surfaces. AFM imaging allowed us to monitor the opening and closing of the nanopores in real time and demonstrate that these phenomena happen on a timescale of seconds, which suggests that the grafting-to in melt of PNIPAAM on suitably designed nanoporous surfaces is an interesting method for the fabrication of thermoactuated nanovalves with a fast response rate.

Future work is aimed at immobilizing smart polymers on ultrathin freestanding nanoporous membranes. These devices can find applications as smart ultrafiltration systems, miniaturized biosensors, and intelligent cell growth platforms or can be incorporated into more complex systems featuring controlled permeability for drug delivery.

Acknowledgment. We acknowledge the funding from the Marie Curie FP6 RTN Biopolysurf. Dr. Jerome Poelesel Maris is gratefully acknowledged for fruitful discussions concerning AFM in liquid media.

Supporting Information Available: XPS spectra and deconvolution of C 1s peaks, calculation of layer thickness from ATR-FT-IR data, and transition-time calculation. This material is available free of charge via the Internet at http://pubs.acs.org.